Clim Dyn (2012) 39:2569–2584
DOI 10.1007/s00382-011-1223-x

Future changes in tropical cyclone activity projected by multi-physics and multi-SST ensemble experiments using the 60-km-mesh MRI-AGCM

Hiroyuki Murakami · Ryo Mizuta · Eiki Shindo

Received: 26 August 2011 / Accepted: 12 October 2011 / Published online: 28 October 2011

Abstract Uncertainties in projected future changes in tropical cyclone (TC) activity are investigated using future (2075–2099) ensemble projections of global warming under the Intergovernmental Panel on Climate Change (IPCC) A1B scenario. Twelve ensemble experiments are performed using three different cumulus convection schemes and four different assumptions for prescribed future sea surface temperatures (SSTs). All ensemble experiments consistently project significant reductions in global and hemispheric TC genesis numbers as well as reductions in TC frequency of occurrence (TCF) and TC genesis frequency (TGF) in the western North Pacific, South Indian Ocean, and South Pacific Ocean. TCF and TGF are projected to increase over the central Pacific which is consistent with the findings of Li et al. (2010). Inter-experimental variations of projected future changes in TGF and TC genesis number are caused mainly by differences in large-scale dynamical parameters and SST anomalies. Thermodynamic parameters are of secondary importance for variations in TGF and TC genesis number. These results imply that differences in SST spatial patterns can cause substantial variations and uncertainties in projected future changes of TGF and TC numbers at ocean-basin scales.

Keywords Tropical cyclones · Global warming · Future projections · High-resolution model · Uncertainties · Ensemble experiments

H. Murakami (✉)
Japan Agency for Marine-Earth Science and Technology (JAMSTEC)/Meteorological Research Institute (MRI), 1-1, Nagamine, Tsukuba, Ibaraki 305-0052, Japan
e-mail: hir.murakami@gmail.com

Present Address:
H. Murakami
International Pacific Research Center, School of Ocean and Earth Science and Technology, University of Hawaii at Manoa, Honolulu, Hawaii, USA

R. Mizuta · E. Shindo
Climate Research Department, Meteorological Research Institute (MRI), 1-1, Nagamine, Tsukuba, Ibaraki 305-0052, Japan
e-mail: rmizuta@mri-jma.go.jp

E. Shindo
e-mail: eishindo@mri-jma.go.jp

1 Introduction

Projections of the potential impacts of global warming on regional tropical cyclone (TC) activity are important for estimations of potential future socio-economic losses. Both theory (Emanuel 1987) and modelling studies (Knutson et al. 2010) suggest that the TC intensity could increase with global warming (IPCC 2007); however, projected changes in the TC genesis number have varied considerably, especially at the ocean-basin scale (IPCC 2007; Emanuel 2008; Zhao et al. 2009; Knutson et al. 2010). This inconsistency among projections arises from a number of factors, including differences in assumed spatial patterns of future changes in sea surface temperature (SST; Sugi et al. 2009; Zhao et al. 2009), differences in model physical parameterisations (Walsh et al. 2010), differences in the chosen global warming scenario (Stowasser et al. 2007), and differences in the methods used to detect TCs (Walsh et al. 2007).

Although some studies have addressed uncertainties due to variations in assumed future changes in SST (Emanuel 2008; Sugi et al. 2009; Zhao et al. 2009), there has been little work that addresses uncertainties that arise from

differences in model physics. Several studies have compared and contrasted results from various World Climate Research Programme's Coupled Model Inter-comparison Project phase 3 (CMIP3) models (e.g., Yokoi et al. 2009; Yokoi and Takayabu 2009; Walsh et al. 2010); however, it is difficult to identify the causes of differences in the projections because the analysed models differ in multiple ways (e.g., model resolutions, dynamical representations, and physical parameterisations).

In this study, we conduct ensemble projections that consider differences in both tropical spatial patterns of SST changes and model physics, particularly the cumulus parameterisation scheme. This approach allows us to address of the relative impacts of differences in projected SST changes and differences in model physics on projected future changes in global and regional TC activity. A key factor in projecting future climate change is to derive robust signals across different model physics and different future SST patterns. Li et al. (2010) examined the sensitivity of future TC projections with various global high-resolution (40–50-km-mesh) models and various future SST patterns. In the present study, we extend this methodology by examining the same model but with different physical packages, forced with different groups of future SST patterns derived from eighteen IPCC Fourth Assessment Report (AR4) coupled models.

The remainder of this paper is organised as follows. Section 2 briefly describes the models, experimental design, and analysis methods. Section 3 presents the results. Section 4 discusses the results in the context of previous work and provides a summary of the conclusions.

2 Methods

2.1 Models

The model used in this study is the Meteorological Research Institute Atmospheric General Circulation Model (MRI-AGCM) version 3.2 (Mizuta et al. 2012). The model simulations are run at a horizontal resolution of T_L319 (equivalent to 60-km-mesh). The model is equipped with multiple cumulus convection schemes, which can be easily switched. In this study, three cumulus convection schemes are used to develop the multi-physics ensemble simulations: a prognostic Arakawa–Schubert (AS) cumulus convection scheme (Arakawa and Schubert 1974; Randall and Pan 1993); a new cumulus convection scheme, called the "Yoshimura scheme (YS)" after a model developer at the MRI (Yukimoto et al. 2011); and a Kain–Fritsch (KF) convection scheme (Kain and Fritsch 1990, 1993). The YS scheme is based on the Tiedtke (1989) scheme, and accounts for multiple detailed entraining and detraining plumes by interpolating two convective updrafts with different rates of turbulent entrainment and detrainment (Yukimoto et al. 2011). The use of the YS scheme in the MRI-AGCM yields a more realistic simulation of tropical precipitation than the use of the AS scheme (Mizuta et al. 2012).

2.2 Lower boundary conditions

The simulation settings and observational datasets are identical to those used in several previous studies (Murakami and Sugi 2010; Murakami and Wang 2010; Murakami et al. 2011). A so-called "time-slice" method (Bengtsson et al. 1996) is applied, in which the high-resolution AGCM is forced by setting the lower boundary conditions to prescribed SSTs. The control realisation is an "AMIP (Atmospheric Model Intercomparison Project)"-style simulation in which the lower boundary conditions are prescribed as observed monthly mean SSTs and sea ice concentrations (SICs) during 1979–2003 according to the Hadley Centre Global Sea Ice and Sea Surface Temperature dataset (HadISST1; Rayner et al. 2003).

The targeted projection window for the future climate is the last quarter of the 21st century (2075–2099). For the SST-ensemble projections, four different projections of future SSTs are prescribed, each of which have a different spatial SST anomaly pattern. One of these patterns is the multi-model ensemble mean of SST computed from future projections by the 18 CMIP3 models under the Special Report on Emission Scenarios (SRES) A1B scenario (IPCC 2007). The other three patterns are created using a cluster analysis, in which normalised tropical SST anomalies derived from the 18 CMIP3 models are grouped to avoid subjective selection of single model. The procedure for the cluster analysis is as follows.

1. For each CMIP3 model, a mean future change in SST is computed by subtracting the 1979–2003 mean SST from the 2075–2099 mean SST.
2. The computed mean future change in SST is normalised by dividing by the tropical mean (30°S–30°N) future change in SST.
3. The normalised value for each model is subtracted from the multi-model ensemble mean of the normalised value.
4. The inter-model pattern correlation r of the normalised values is computed between each pair of models.
5. Norms (or distances) are defined as $2 \times (1 - r)$ for each model, and the cluster analysis is performed using these norms. A small distance between two models indicates they share similar spatial patterns in future changes in tropical SST. Clustering is based on the *Single-linkage* (or minimum-distance) method (Wilks 2006), in which the smallest distance between two models (or groups) is joined step-by-step. When the

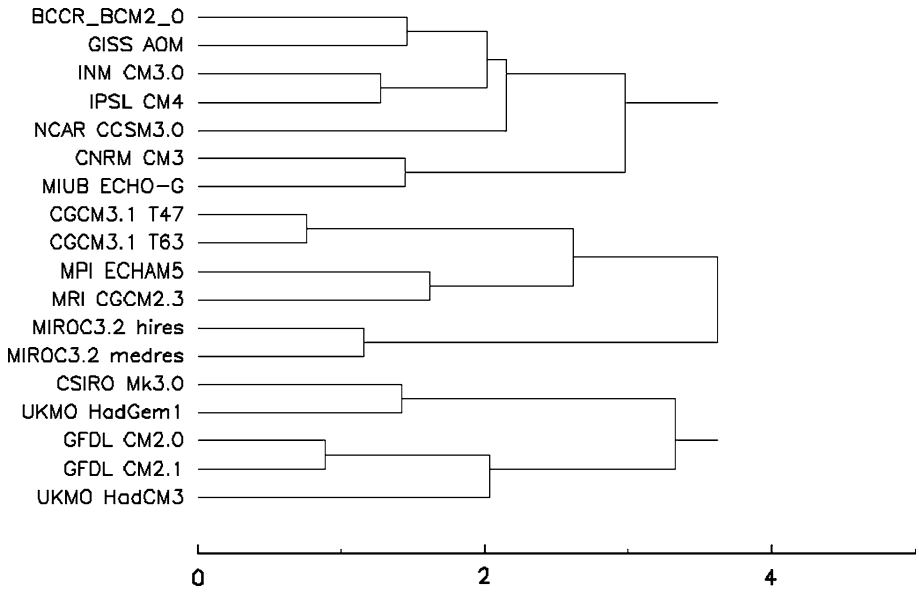

Fig. 1 Dendrogram for clustering of SSTs projected by the 18 CMIP3 models. The results of 15 clustering steps are indicated as the original 18 models are progressively joined from the *left* to the *right* of the diagram. The distances between joined clusters are indicated by the lengths of *horizontal lines*

Table 1 Eighteen CMIP3 models used for cluster analysis

Name	Institute
BCCR_BCM2_0	Bjerknes Centre for Climate Research, Norway
CGCM3.1 T47	Canadian Centre for Climate Modeling and Analysis, Canada
CGCM3.1 T63	
CNRM CM3	Météo-France/Center National de Recherches Météorologiques, France
CSIRO Mk3.0	CSIRO Atmospheric Research. Australia
GFDL CM2.0	Geophysical Fluid Dynamics Laboratory/NOAA/US, Dept. of Commerce, United States
GFDL CM2.1	
GISS AOM	Goddard Institute for Space Studies, National Aeronautics and Space Administration, United States
INM CM3.0	Institute for Numerical Mathematics, Russia
IPSL CM4	Institute Pierre Simon Laplace, France
MIROC3.2 hires	Center for Climate System Research (University of Tokyo), National Institute for Environmental Studies, and Frontier Research Center for Global Change (JAMSTEC), Japan
MIROC3.2 medres	
MIUB ECHO-G	Meteorological Institute of the University of Bonn, Meteorological Research Institute of KMA, and Model and Data Group, Germany and Korea
MPI ECHAM5	Max Planck Institute for Meteorology, Germany
MRI CGCM2.3	Meteorological Research Institute, Japan
NCAR CCSM3.0	National Center for Atmospheric Research, United States
UKMO HadCM3	Hadley Centre for climate prediction and research/Met Office, United Kingdom
UKMO HadGeml	

final three groups are bounded, the clustering procedure is terminated.

Figure 1 shows a dendrogram, reflecting the clustering of the 18 CMIP3 models listed in Table 1. Each cluster consists of five or seven models. Only three cluster groups are identified, because a greater number of groups would increase the risk that the results would be dominated by a single outlier model.

Detrended observed interannual variations are added to the computed future anomalies (see Mizuta et al. 2008 for the details), with the assumption that interannual variations of SSTs in the future projection are similar to those of the present-day. Figure 2 shows all four prescribed future changes in the annual-mean SST. Note that SST warming in the CMIP3 ensemble mean (Fig. 2a) is spatially inhomogeneous (Xie et al. 2010): a greater warming occurs in the northern tropics than in the southern tropics.

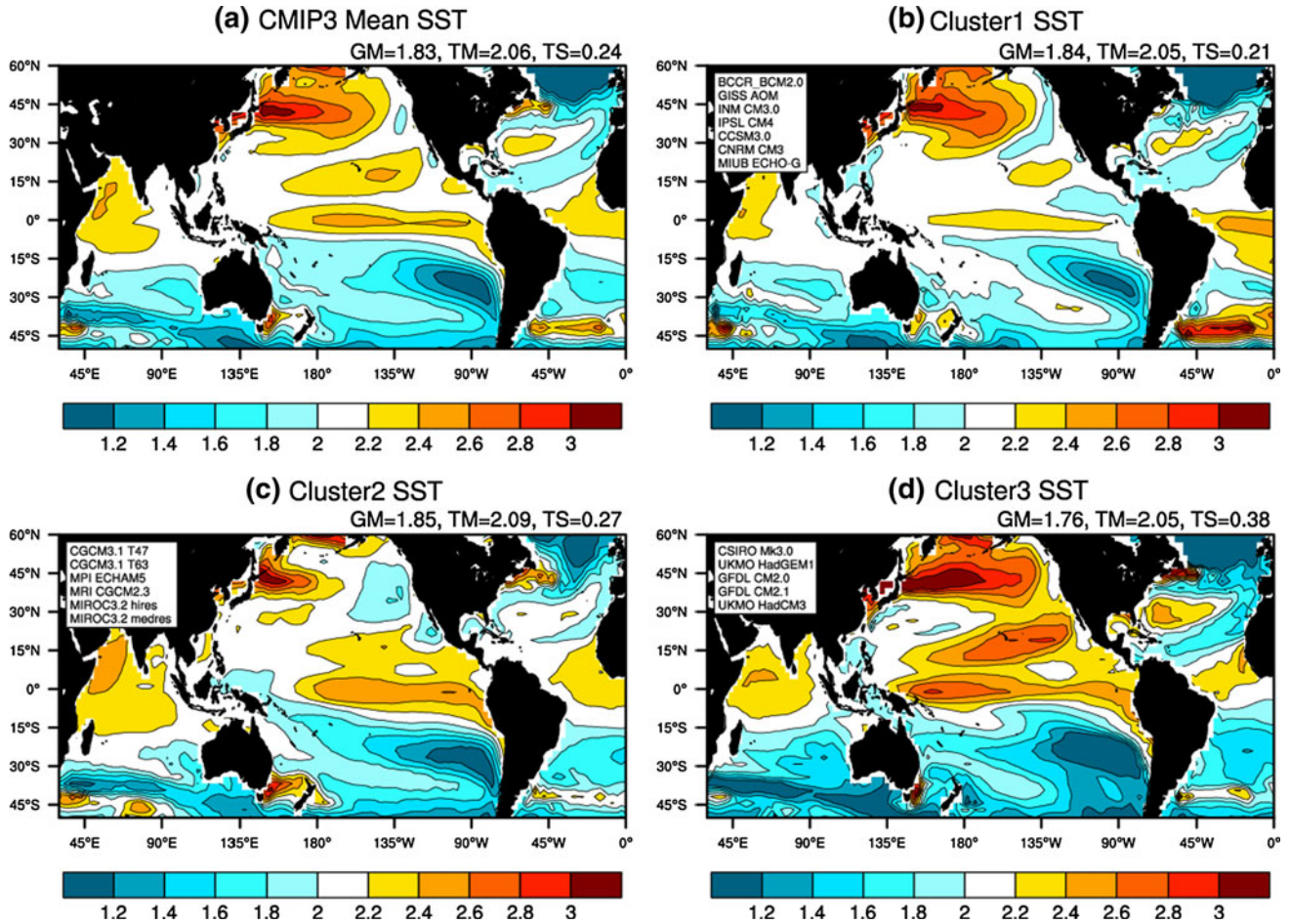

Fig. 2 Annual means of prescribed future changes in sea surface temperatures (SSTs) [°C]. **a** Ensemble mean of 18 CMIP3 models. **b–d** Changes in SSTs classified using a cluster analysis. The numbers at the *top right* of each panel show the global mean SST change (GM), tropical (30°S–30°N) mean SST change (TM), and standard deviation of the tropical SST spatial change (TS), respectively. The models listed in the *top left* corner of each panel identify the CMIP3 models grouped in that cluster

The greatest SST warming occurs in the tropical and subtropical central Pacific, tropical Atlantic, and tropical Indian Ocean. The three grouped cluster SSTs are shown in Fig. 2b–d. Cluster 1 (Fig. 2b) shows less warming over the central Pacific relative to the CMIP3 ensemble mean and the other clusters, so that the spatial variation in the tropics is small. Cluster 2 (Fig. 2c) is similar to the CMIP3 ensemble mean, but with greater warming in the Indian Ocean than the other prescribed SSTs. Cluster 3 (Fig. 2d) has the largest spatial variation in the tropics among all of the prescribed SSTs, and shows relatively large warming of SSTs in the tropical western Pacific and subtropical central Pacific.

In all, 12 ensemble simulations are conducted (3 cumulus schemes × 4 projected future patterns of SSTs). Table 2 lists all of the experiments. An additional simulation that assumes a globally uniform projected SST change of +1.83 K (the global mean SST increase between 1979–2003 and 2075–2099) is also conducted for comparison with the experiments in which SST changes vary spatially. The YS convection scheme is used in this additional simulation. For convenience, the abbreviations listed in Table 2 will be used throughout the remainder of this paper to refer to the experiments.

2.3 Observational dataset

The TC climatology for the control simulations is validated using the global TC dataset compiled on the Unisys Corporation website (Unisys 2012). This dataset consists of best-track TC data provided by the National Hurricane Center (NHC) and Joint Typhoon Warning Center (JTWC), and contains historical TC information, such as the location, intensity (maximum 1-min surface wind speed), and central sea level pressure (SLP) of TCs at 6-h intervals from 1851 to 2011 (note that the record period is basin-dependent). This study considers only TCs of tropical storm intensity or stronger (i.e., TCs that possess 1-min

Table 2 List of ensemble future projections

Abbreviation	Cumulus convention scheme	Prescribed future SST
Y0	Yoshimura Scheme (YS)	18 CMIP3 models ensemble mean
Y1	Yoshimura Scheme (YS)	Cluster 1
Y2	Yoshimura Scheme (YS)	Cluster 2
Y3	Yoshimura Scheme (YS)	Cluster 3
K0	Kain-Fritsch Scheme (KF)	18 CMIP3 models ensemble mean
K1	Kain-Fritsch Scheme (KF)	Cluster 1
K2	Kain-Fritsch Scheme (KF)	Cluster 2
K3	Kain-Fritsch Scheme (KF)	Cluster 3
A0	Arakawa-Shubert Scheme (AS)	18 CMIP3 models ensemble mean
A1	Arakawa-Shubert Scheme (AS)	Cluster 1
A2	Arakawa-Shubert Scheme (AS)	Cluster 2
A3	Arakawa-Shubert Scheme (AS)	Cluster 3

sustained surface wind speeds of 35 kt or greater) between 1979 and 2003.

2.4 Detection algorithm for tropical cyclones

TCs are detected in the model by evaluating 6-hourly model outputs using globally uniform criteria. These criteria are based on those described by Oouchi et al. (2006), but with some modifications (Murakami et al. 2012). Some criteria are optimised for a given model configuration to ensure that the present-day global annual mean TC number matches that observed (about 84 per year for the period 1979–2003). The values listed in parentheses after each of the following criteria show the model-dependent values used for the optimisation (from left, values are for experiments using YS, KF, and AS convection schemes, respectively).

1. The maximum relative vorticity at 850 hPa exceeds (8.0×10^{-5}, 2.1×10^{-4}, and 1.0×10^{-5}) s^{-1}.
2. The maximum wind speed at 850 hPa exceeds (13.0, 22.0, and 11.5) m s^{-1}.
3. There is an evident warm core aloft. Namely, the sum of the temperature deviations at 300, 500, and 700 hPa exceeds (0.8, 2.0, and 0.5) K. The temperature deviation for each level is computed by subtracting the maximum temperature from the mean temperature over the $10° \times 10°$ grid box centred nearest to the location of maximum 850 hPa vorticity.
4. The maximum wind speed at 850 hPa is greater than the maximum wind speed at 300 hPa.
5. To remove tropical depressions in the North Indian Ocean (NIO), the radius of maximum mean wind speed must be less than 200 km from the detected storm centre. This condition is applied in the NIO only.
6. The duration of each detected storm must exceed 36 h. To prevent double TC counts arising from detection and termination within a single 6-h time step, termination during a single time step is allowed.

Note that the model-dependent detection thresholds are highly variable, reflecting differences in the mean TC intensity among the cumulus convection schemes. Figure 3 shows observed TC tracks and intensities along with the distributions of TC tracks and intensities simulated by the control model configurations. The YS and KF control simulations perform better in capturing the observed distribution and intensity of TCs than does the AS control simulation. Murakami et al. (2012) considered the reason why the YS and KF schemes simulate more intense TCs than does the AS scheme. Briefly, convective heating is more tightly constrained in the YS and KF schemes, which appears to induce intense grid-scale upward motions and to promote large-scale condensation, resulting in the development of a more intense TC.

Criterion (5) is necessary because we found that monsoon depressions in the North Indian Ocean may be erroneously detected as TCs during the monsoon season regardless of the other detection criteria. Monsoon depressions have some characteristics in common with TCs. The monsoon depression in the North Indian Ocean is a cyclonic low-pressure system that forms within the monsoon trough during the monsoon season, characterized by (1) a large horizontal scale of 2,000–3,000 km; (2) maximum wind speeds located at more than 200 km from the centre of the system; and (3) a low vertical structure that extends up to 8 km (Ding and Sikka 2006). The effects of strong wind shear mean that monsoon depressions never develop into a TC during the monsoon season; hence, the use of another criterion, based on vertical wind shear, may be able to distinguish between monsoon depressions and TCs.

All models tend to underestimate TC numbers in the North Atlantic, and overestimate TC numbers in the Southern Hemisphere. These model biases should be taken into account for meaningful projections of future changes in TC activity. The future changes for each ensemble simulation are computed by taking the difference between each individual future projection and its related control simulation, implying that model biases could be inherited

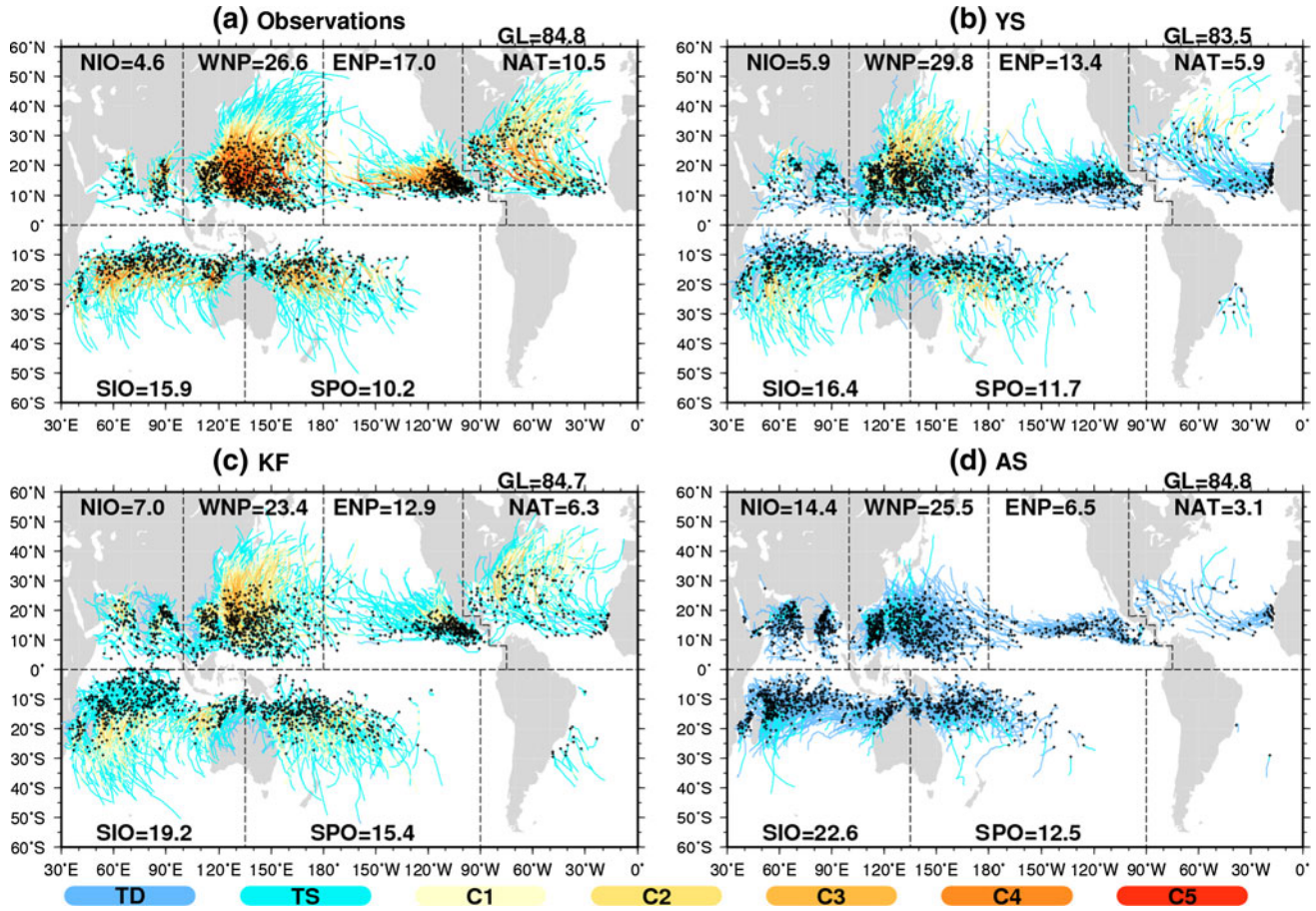

Fig. 3 Global distribution of tropical cyclone (TC) tracks during all seasons from 1979 to 2003 according to **a** observations, **b** the control simulation using Yoshimura (YS) convection scheme, **c** the control simulation using the Kain–Fritsch (KF) convection scheme, and **d** the control simulation using the Arakawa–Schubert (AS) convection scheme, respectively. *Black dots* are TC genesis locations. The numbers printed for each ocean basin indicate the annual mean number of TCs in that basin. TC tracks are coloured according to the intensity of the TC, as categorized by the Saffir–Simpson Hurricane Wind Scale (e.g., tropical depression (TD), tropical storms (TS), and the Categories 1–5 (C1-C5))

by projections of future change. Model performance should be optimized for most reliable future projections; however, all the models are considered here both to show how models using different cumulus schemes respond to the same changes in SST, and to identify points of consistency in the different future projections.

TC positions are counted for each 2.5° × 2.5° grid box within the global domain at 6-hourly intervals. The TC frequency (TCF) is defined as the total count for each grid box. The location of TC genesis is defined as the position at which the TC is first detected, and the TC genesis frequency (TGF) is defined similarly to TCF. Because the computed frequency fields are noisy, they are smoothed using a weighted 9-point average, for which the weights depend on distance from the centre of the grid box. The results of this study are robust even if 5.0° × 5.0° grid boxes are used instead of 2.5° × 2.5° grid boxes.

Nine ocean basins are considered in this analysis: global (GL), Northern Hemisphere (NH), Southern Hemisphere (SH), North Indian Ocean (NIO), Western North Pacific (WNP), Eastern North Pacific (ENP), North Atlantic (NAT), South Indian Ocean (SIO), and South Pacific Ocean (SPO) (see Fig. 3 for regional boundaries).

3 Results

3.1 Projected future changes in TC genesis number

Figure 4 shows projected fractional future changes in TC genesis number for each ensemble experiment. The projected global TC numbers are significantly reduced in the future climate projections by amounts ranging from 5 to 35%. The standard deviations of the projected fractional future changes are small (about 5%), indicating that the reductions in TC numbers at the global scale are robust among these experiments. Cluster 3 SST experiments show slightly smaller reductions than the other SST experiments

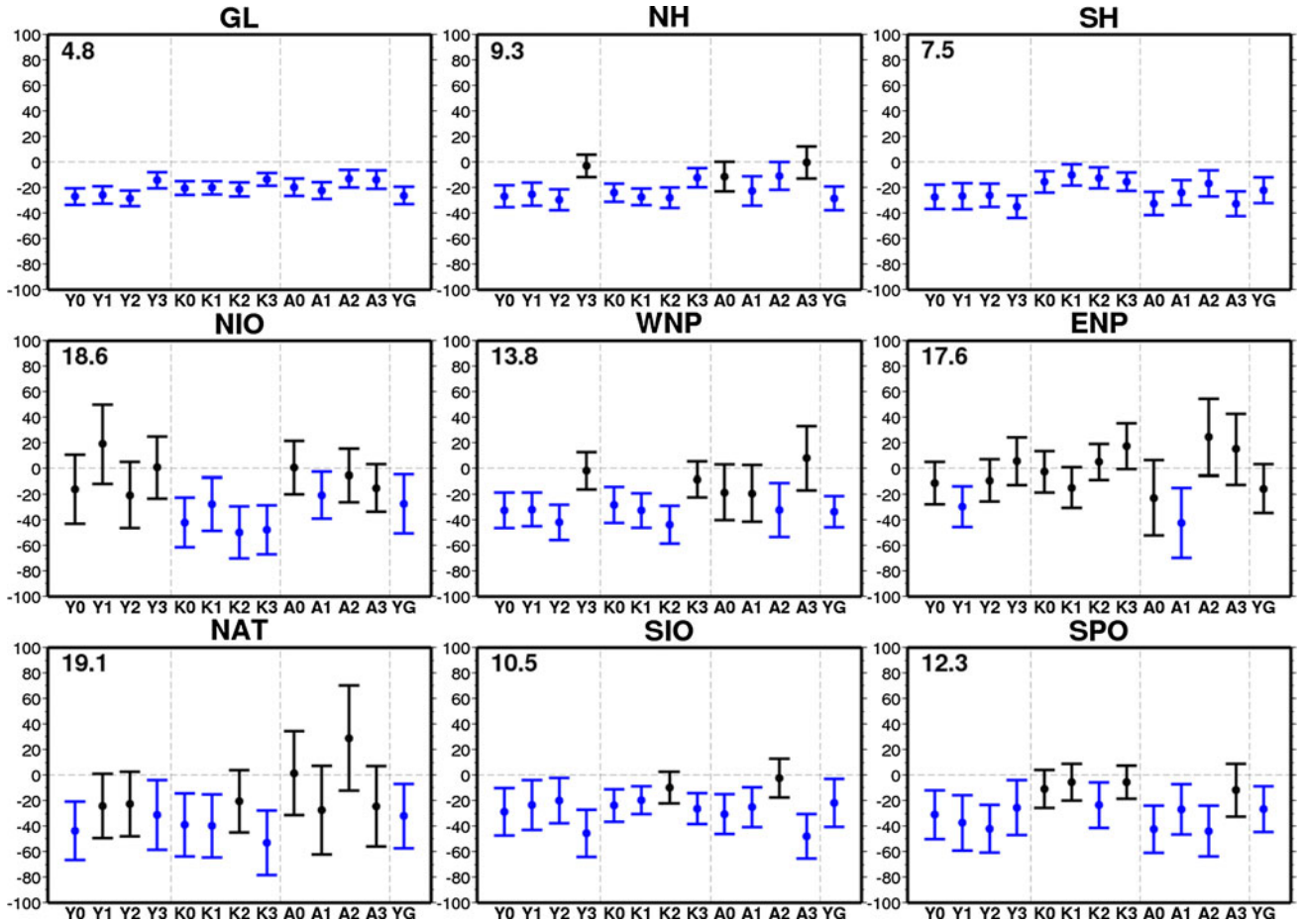

Fig. 4 Fractional future changes [%] in TC genesis number for each basin according to each ensemble experiment. The *error bars* indicate 90% confidence intervals. *Blue bars* indicate that projected future changes that are statistically significant at 90% level according to the two-sided Student's *t* test. YG is an additional experiment forced by a globally uniform change in SST of +1.83 K relative to the present-day. The number in the *top left* corner of each panel shows the standard deviation of twelve ensemble experiments (i.e., YG experiment is not included)

for all three cumulus convection schemes. The number of TCs is also projected to decrease significantly at the hemispheric scale by most of the experiments; however, the Cluster 3 experiments show relatively smaller decreases in NH and relatively larger decreases in the SH than the other experiments. These results indicate that projections of future changes in TC numbers depend to some extent on the spatial pattern of prescribed SST changes.

The majority of the experiments show reductions in projected TC numbers in WNP, SIO, and SPO. Changes in TC numbers in other basins vary substantially among the experiments, in both sign and amount. Variations caused by different SSTs appear to be larger than those caused by different cumulus schemes in WNP, ENP, and SIO, indicating that uncertainties in projected SST spatial patterns introduce uncertainties in future changes in TC numbers in these basins. In NIO, NAT, and SPO, on the other hand, changes in TC numbers appear to depend on the choice of cumulus convection scheme, indicating that differences in model representations of physical processes may also be an important source of uncertainty.

Projected future reductions in TC numbers at the global and hemispheric scales appear to be robust among the experiments; however, changes in individual ocean basins vary substantially with different prescribed SST spatial patterns and cumulus convection schemes. These regional discrepancies underscore continuing uncertainties regarding how TC activity is likely to change at the basin-scale.

3.2 Projected future changes in TCF and TGF

Figure 5 shows ensemble mean projected future changes in the spatial distributions of TCF and TGF. Locations where these changes are robust (i.e., the mean future change is statistically significant at the 90% confidence level and changes in more than 10 out of 12 individual experiments are

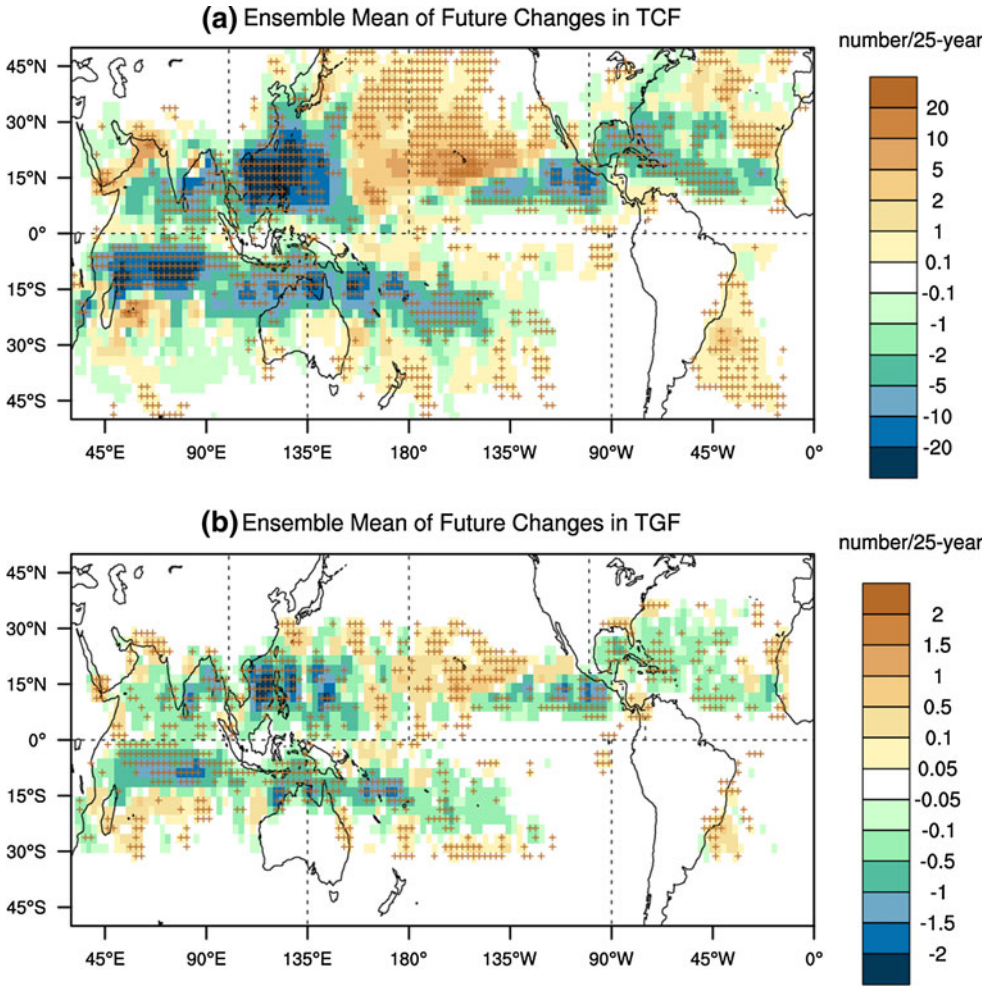

Fig. 5 Ensemble mean future changes in **a** tropical cyclone frequency (TCF) and **b** tropical cyclone genesis frequency (TGF) [number/25-years]. *Cross marks* indicate that the differences are statistically significant at the 90% confidence level or above according to the two-sided Student's *t* test and that more than 10 experiments (approximately 80% of all ensemble experiments) project mean changes of the same sign

of the same sign as the mean future change) are marked with crosses. Both TCF and TGF are projected to decrease significantly and robustly in the western WNP, eastern ENP, western NAT, SIO, and SPO, and both quantities increase significantly in the central Pacific. This latter result indicates a potential future increase in TC-related economic damage in the Hawaiian region. TC genesis is also projected to shift poleward in the both hemispheres in the future climate.

As described in Sect. 3.1, the projected TC number varies significantly with the different prescribed spatial patterns of future SST in the WNP, ENP, and SIO ocean basins. Figure 6 shows the ensemble mean of future changes in TGF and SST anomaly (S_a) averaged for experiments with either the same SST or the same cumulus convection scheme. The S_a is computed by subtracting the tropical mean (30°S–30°N) change in SST from the local change in SST. Locations where S_a increases substantially show large increases in TGF as well. For example, relatively large increases in TGF occur in the Cluster 3 SST ensemble (Fig. 6d) in both the central Pacific and subtropical central Pacific, where S_a is also substantially increased. This positive correlation between maximum S_a and positive TGF anomaly has also been reported in recent studies of future climate projections (Sugi et al. 2009; Zhao et al. 2009) and present-day seasonal predictions (Zhao et al. 2010) over NAT. Reductions in TGF are not necessarily collocated with minima in S_a, however: none of the substantial projected decreases in TGF over WNP, SIO, and SPO appear to be related to minima in S_a. This decoupling of S_a minima and TGF causes the global pattern correlation between the two quantities to be small, despite the strong correlation between S_a maxima and TGF. An additional experiment, for which the prescribed change in SST is globally uniform (Fig. 6h), projects a similar spatial pattern of future changes in TGF to that of the ensemble mean (Fig. 5b), with substantial decrease in TGF in the WNP, eastern ENP, SIO, and SPO, and an increase over the central Pacific. This indicates that the basic spatial pattern of projected TGF changes is formed by the underlying global warming. Local positive S_a appears to add a positive TGF anomaly in the underlying changes in TGF spatial pattern.

Figure 6e–g compares ensemble experiments using different convective schemes. Differences among experiments with different cumulus convection schemes are small,

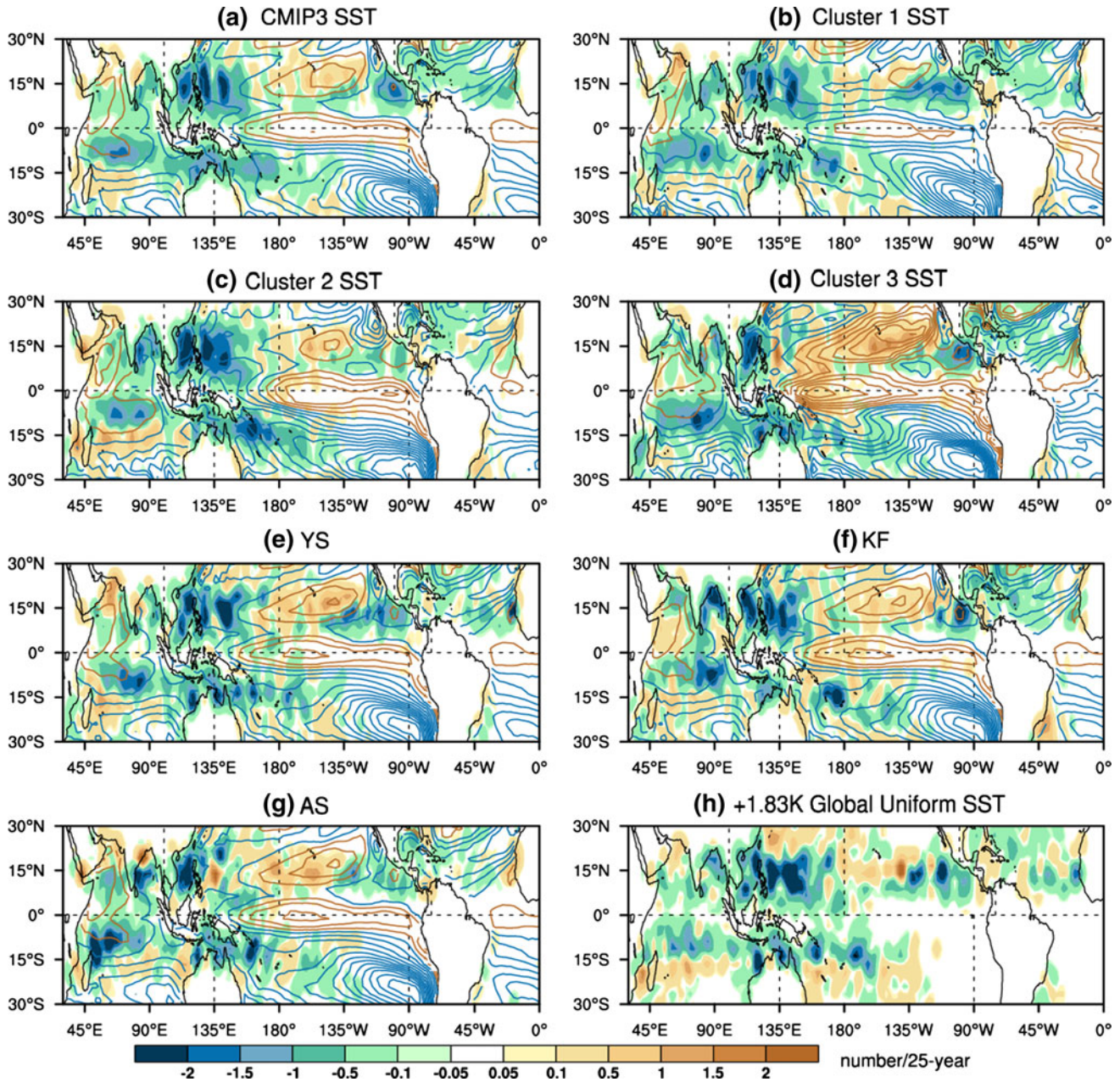

Fig. 6 Ensemble mean future changes in tropical cyclone genesis frequency (TGF, shading) [number/25-years] and sea surface temperature anomaly (S_a, contours) [K] relative to tropical (30°S–30°N) mean. *Red* (*blue*) coloured contours indicate S_a of more (less) than 0.2 K, with a contour interval of 0.1 K. Each *panel* shows the ensemble mean of **a** CMIP3 SST experiments, **b** Cluster 1 SST experiments, **c** Cluster 2 SST experiments, **d** Cluster 3 SST experiments, and experiments using **e** Yoshimura convection scheme (YS), **f** Kain–Fritsch (KF) convection scheme, and **g** Arakawa–Schubert (AS) convection scheme. **h** Future change in TGF according to an additional experiment forced by a globally uniform change in SST of +1.83 K relative to the present-day

indicating that projected future global changes in TGF are largely independent of the chosen cumulus convection scheme in the MRI-AGCM.

3.3 Future changes in large-scale parameters

In addition to S_a, several other factors may possibly be associated with TC genesis frequency. A number of previous studies have reported relationships between large-scale dynamical and thermodynamic parameters, and variations in TC genesis (Gray 1968; Emanuel and Nolan 2004). The response of large-scale atmospheric parameters may vary with differences in the model physics, even if the prescribed SST is the same. This section examines the extent to which projected future changes in TGF can be explained by large-scale parameters, as well as how much

projected future changes in these large-scale parameters vary among the ensemble experiments.

The analysed large-scale parameters were identified by Emanuel and Nolan (2004), and are known collectively as Genesis Potential Index (GPI): relative vorticity at 850 hPa (η_{850}), relative humidity at 700 hPa (RH), maximum potential intensity ($V_{\rm pot}$; Emanuel 1995), and vertical wind shear between 200 and 850 hPa (V_s). In addition to the GPI factors, Murakami and Wang (2010) and Murakami et al. (2011) suggested that vertical pressure–velocity at 500 hPa (ω_{500}) is necessary to reflect projected future changes in TGF. Emanuel (2008) suggested that saturation deficit in the lower troposphere may be related to future changes in TC genesis numbers. The saturation deficit is defined in this study as

$$\chi \equiv e_w - e = e_w\left(1 - \frac{RH}{100}\right) \quad (1)$$

where χ is the saturation deficit [Pa], e_w is the saturation vapour pressure, e is the actual vapour pressure, and RH is relative humidity at 700 hPa. Sugi et al. (2002) and Bengtsson et al. (2007) further suggested that an increase in atmospheric static stability could cause a decrease in the global TC frequency, where static stability (Γ_d) is defined as the difference in potential temperature between 200 and 850 hPa. Li et al. (2010) suggested that variance of synoptic scale disturbances (D; Lau and Lau 1990), which is defined as the variance of 2–8-days band-pass filtered 850 hPa vorticity, could also explain projected future changes in TGF. Vertical easterly shear favours the development of synoptic-scale disturbances (Wang and Xie 1996; Li 2006). Vertical zonal-wind shear (V_{zs}) is defined as the difference in zonal wind between 200 and 850 hPa (i.e., negative values indicate easterly shear, which is favourable for low-level disturbances). These parameters are correlated with and depend upon each other to varying degrees. Furthermore, because TC existence may affect the monthly mean fields in regions where TCF is large, grid cells with values of TCF greater than 3.0 have been removed from monthly mean data prior to calculation of the climatological monthly means. Following Held and Zhao (2011), the relevance of these large-scale parameters to the projected future changes in TGF is examined by computing the climatological mean field of the filtered large-scale parameter, weighting the 12 climatological months by the sum of TGF in the control simulation and future projection for each 2.5° × 2.5° grid box as:

$$[A(x,y)]_G \equiv \frac{\sum_{t=1}^{12} G_t(x,y)A_t(x,y)}{\sum_{t=1}^{12} G_t(x,y)} \quad (2)$$

where (x, y) describes the location of the grid box, t is the month, A_t is the climatological monthly mean of a large-scale parameter for the month t, and G_t is the climatological monthly mean TGF summed over both the control and future experiments for the month t. Weighting the climatological mean by TGF reduces the effects of months during which TC genesis seldom occurs on the mean field. G_t varies according to the pair of present and future experiments. The results of this study are generally robust even if G_t is fixed as a summation of monthly TGFs for all present and future experiments.

Figure 7 shows ensemble mean spatial distributions for the large-scale parameters. The global pattern correlation between the plotted quantity and projected TGF are shown in the bottom right corner of each panel in Fig. 7, and the basin-scale pattern correlations are listed in Table 3. The global pattern correlations are quite low, with values of approximately 0.33 at most. The dynamical factors of η_{850}, ω_{500}, and D are more highly correlated with projected changes in TGF than the thermodynamic parameters, with the exception of Γ_d. This implies that future changes in dynamical factors are more influential than future changes in thermodynamic factors in determining future changes in the spatial pattern of TGF. The highest pattern-correlation field with the ensemble mean future change in the TGF pattern is D, thereby supporting the argument that D is a major field that differentiates the distinctive regional characteristics of projected TC changes (Li et al. 2010; Li 2011). The spatial distribution of D is strongly correlated with that of V_{zs} (Li et al. 2010), except for NAT and SIO, indicating that the activity of synoptic-scale disturbances will be enhanced in easterly-shear-anomaly regions in the future. The increase in easterly vertical wind shear in the central Pacific may be due to the increase in diabatic heating in the central and eastern Pacific (as seen in ω_{500} in Fig. 7i) which is accompanied by an increase in S_a (Fig. 7a). In turn, the increase in diabatic heating induces low-level convergence (i.e., westerly flow) and upper-level divergence (i.e., easterly flow) over the central Pacific, resulting in an increase in the easterly vertical wind shear (Li et al. 2010). The spatial distribution of η_{850} (Fig. 7f) also appears to be related to that of diabatic heating through the Rossby wave response (Gill 1980; Murakami et al. 2011); i.e., cyclonic vorticity anomalies appear at the northwest (southwest) flank of upward motion anomalies in the NH (SH).

Tripole spatial patterns are apparent in NAT for most variables, which is consistent with the findings of Vecchi and Soden (2007b) and Murakami and Wang (2010); however, these spatial patterns are not well correlated with the ensemble mean TGF pattern (Fig. 5b), resulting in small spatial correlation coefficients in NAT (Table 3). The reason for these weak correlations is unclear, although they may relate to the large biases in TC climatology in the control simulations (Fig. 3).

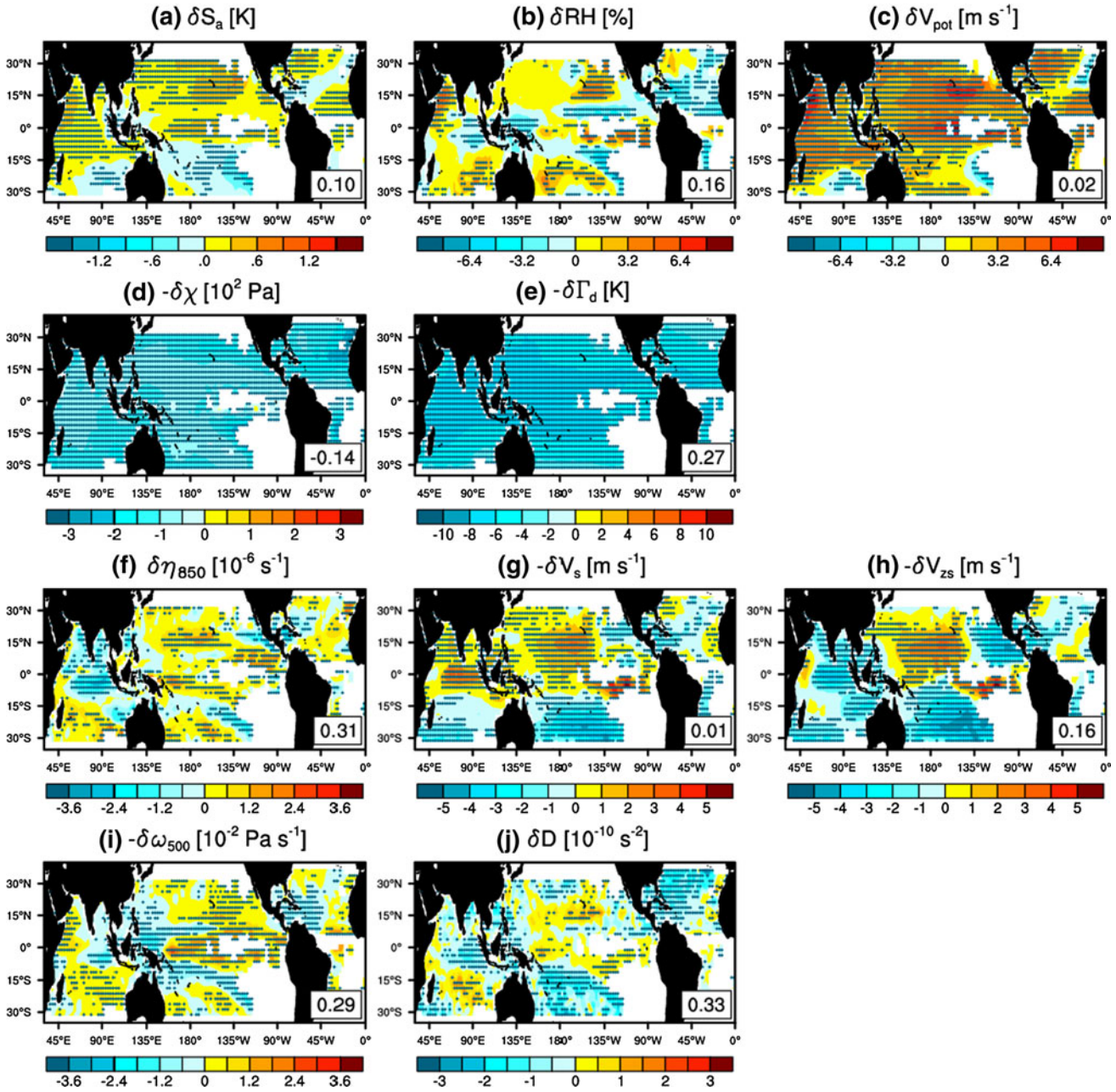

Fig. 7 Future changes in large-scale weighted parameters according to the full ensemble mean: **a** SST anomaly [K], **b** relative humidity at 700 hPa [%], **c** maximum potential intensity [m s^{-1}], **d** saturation deficit at 700 hPa [10^2 Pa], and **e** static stability [K] for thermodynamic parameters, and **f** relative vorticity at 850 hPa [10^{-6} s^{-1}] (positive values indicate cyclonic), **g** *vertical* wind shear [m s^{-1}], **h** *vertical* zonal wind shear [m s^{-1}], **i** *vertical* pressure–velocity at 500 hPa [10^{-2} Pa s^{-1}], and **j** synoptic-scale disturbances [10^{-10} s^{-2}] for dynamical parameters. The number in the *bottom right* corner of each *panel* shows the spatial correlation coefficient between the plotted quantity and the projected changes in TGF shown in Fig. 5b. *Cross marks* indicate ensemble-mean differences that are consistent among more than 10 experiments (approximately 80% of all ensemble experiments)

A near-zero pattern correlation between V_{pot} and Fig. 5b suggests that this thermodynamic factor, which is primarily determined by the future SST pattern, does not determine the future regional-scale TC projection. Other thermodynamic parameters, such as χ (Fig. 7d) and Γ_d (Fig. 7e), are spatially homogeneous relative to dynamical parameters with negative values, indicating that these thermodynamic parameters are of secondary importance in controlling spatial variations in TGF changes.

Among the ocean basins, correlations between TGF and each large-scale parameter are relatively high in WNP and ENP. In particular, although the correlation between TGF

Table 3 Pattern correlations between ensemble mean of projected future changes in large-scale parameters and tropical cyclone genesis frequency (TGF) in different TC basins (Fig. 5b)

	Thermodynamic					Dynamic				
	δS_a	δRH	δV_{pot}	$-\delta\chi$	$-\delta\Gamma_d$	$\delta\eta_{850}$	$-\delta V_s$	$-\delta V_{zs}$	$-\delta\omega_{500}$	δD
GL	**0.10**	**0.16**	0.02	−0.14	**0.27**	**0.31**	0.01	**0.16**	**0.29**	**0.33**
NH	**0.32**	**0.17**	**0.16**	−0.15	**0.24**	**0.25**	**0.15**	**0.24**	**0.31**	**0.41**
SH	−0.11	**0.16**	−0.14	−0.13	**0.32**	**0.39**	−0.11	0.08	**0.27**	**0.24**
NIO	**0.35**	**0.25**	**0.34**	−0.18	**0.29**	**0.26**	0.07	0.15	**0.41**	**0.40**
WNP	**0.45**	0.05	**0.33**	−0.24	**0.19**	**0.45**	**0.47**	**0.25**	**0.28**	**0.48**
ENP	**0.32**	**0.43**	**0.24**	−0.07	**0.20**	**0.19**	**0.32**	**0.56**	**0.15**	**0.54**
NAT	−0.11	0.13	−0.30	−0.12	0.09	**0.28**	0.10	0.12	**0.26**	**0.23**
SIO	−0.43	**0.34**	−0.37	−0.29	**0.36**	**0.48**	−0.31	0.07	**0.25**	**0.29**
SPO	**0.14**	**0.14**	0.10	−0.08	**0.26**	**0.30**	0.08	0.12	**0.35**	**0.35**

Bold numbers indicate positive correlations that are statistically significant at the 99% level according to Pearson's product-moment correlation significant test

and the SST anomaly S_a is low in GL, it correlates with TGF stronger in the WNP and ENP than in the global scale. This result indicates that S_a may substantially influence TGF in the central Pacific.

3.4 Variance among the ensemble experiments

Inter-experimental correlation coefficients between the fractional changes in total TGF and future changes in weighted large-scale parameters are calculated for each basin to evaluate whether differences in model physics or prescribed SST distributions are responsible for total variance in the future changes in TGF and large-scale parameters (Table 4). Scatter plots between projected fractional changes in total TGF and mean future changes in large-scale parameters are also shown in Fig. 8 (some thermodynamic parameters, NH, and SH are not shown). Among the parameters, only S_a is significantly positively correlated globally. S_a and projected changes in TGF are also highly correlated for WNP, ENP, and SIO; these high basin-scale correlations appear to cause the high global-scale correlation in turn. In addition to S_a, there are some dynamical parameters (e.g., η_{850}, V_{zs}, ω_{500}, and D) that are significantly correlated with TGF changes in some ocean basins. The correlations between thermodynamic parameters (e.g., RH, χ, and Γ_d) and changes in TGF are relatively low, indicating these thermodynamic parameters are of secondary importance for the inter-experimental differences. Moreover, the relationships between these parameters and TGF are strongest in WNP and ENP, consistent with the idea that these parameters are also well correlated with TGF changes in terms of their spatial distributions in these basins (Fig. 7; Table 3).

The experiments with identical prescribed SSTs are eccentrically located in the panels of Fig. 8 that indicate significant positive correlations, indicating that the large-scale parameters are more heavily influenced by differences in the SST spatial patterns than by differences in the cumulus convection schemes. Figure 9 shows the results of a two-way analysis of variance (ANOVA) without replication (Storch and Zwiers 1999). This analysis reveals the relative contributions of the variances induced by differences in prescribed SST spatial patterns and by differences in the cumulus convection schemes to the total variance. The method decomposes total variance into variance caused by difference in prescribed SSTs, variance caused by differences in the cumulus convection schemes, and residual variance. The method includes a significance test that verifies whether the mean value is affected by the differences in SSTs or cumulus convection schemes. For the TC number (Fig. 9f) and total TGF (Fig. 9l), variances induced by differences in prescribed SSTs (red bars) are generally larger than those induced by differences in the cumulus convection schemes (blue bars). This result indicates that difference in SSTs exert a larger impact on variance in projected future changes in TC genesis. Dynamical factors (e.g., Fig. 9g–k) that are highly correlated with TGF changes (Table 4) also appear to be more heavily influenced by differences in prescribed SSTs than by differences in the cumulus convection schemes. Future changes in thermodynamic parameters (e.g., Fig. 9a–e) with exception of S_a, appear to be heavily dependent on the cumulus convection parameterisation, but these thermodynamic parameters are poorly correlated with the TGF changes (Table 4). Differences in the SST spatial patterns of prescribed SST appear to be more responsible for variability in the degree of future changes in TGF and TC

Table 4 Inter-experimental correlations between fractional changes in TGF [%] and the projected future changes in the climatological means of weighted parameters for different TC basins

	Thermodynamic					Dynamic				
	δS_a	δRH	δV_{pot}	$-\delta\chi$	$-\delta\Gamma_d$	$\delta\eta_{850}$	$-\delta V_s$	$-\delta V_{zs}$	$-\delta\omega_{500}$	δD
GL	**0.70**	−0.22	0.15	0.13	−0.66	0.22	−0.31	−0.28	−0.36	0.08
NH	**0.75**	0.24	**0.74**	0.41	−0.70	**0.53**	**0.69**	0.44	0.15	0.40
SH	0.47	−0.27	−0.06	−0.21	−0.04	**0.60**	**0.64**	0.43	**0.69**	−0.03
NIO	−0.48	0.33	0.31	0.40	−0.14	0.33	−0.81	0.44	−0.39	0.34
WNP	**0.66**	0.06	−0.06	0.23	−0.78	**0.78**	0.49	**0.68**	**0.63**	**0.61**
ENP	**0.64**	−0.00	**0.58**	−0.11	−0.43	**0.51**	**0.72**	**0.51**	**0.51**	**0.62**
NAT	−0.00	0.48	0.22	**0.59**	−0.65	0.43	0.41	**0.50**	−0.29	**0.78**
SIO	**0.71**	0.40	**0.50**	0.28	−0.47	**0.91**	**0.83**	**0.83**	**0.83**	0.40
SPO	0.45	−0.78	−0.21	−0.52	−0.31	0.35	−0.42	−0.10	**0.57**	0.43

Bold numbers indicate positive correlations that are statistically significant at the 90% level or above according to Pearson's product-moment correlation significant test

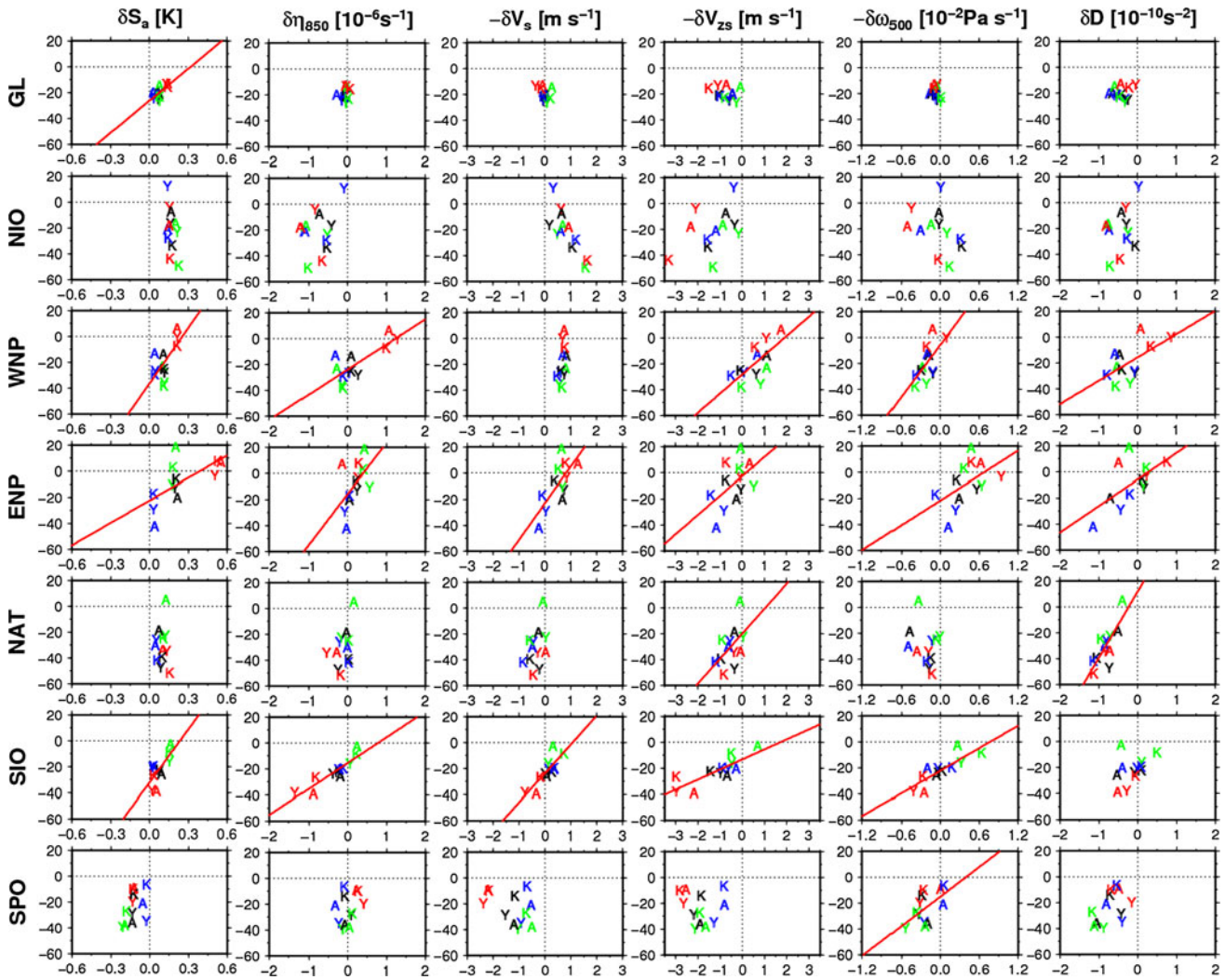

Fig. 8 Scatter diagrams of fractional future changes in tropical cyclone genesis frequency (TGF) [%] as a function of large-scale parameters for each ocean basin. The symbols Y, K, and A indicate experiments using the Yoshimura (YS), Kain–Fritsch (KF), and Arakawa–Schubert (AS) convection schemes, respectively. *Black symbols* represent experiments using CMIP3 ensemble mean sea surface temperature (SST) changes, *blue* symbols represent experiments using Cluster 1 SST changes, *green* symbols represent experiments using Cluster 2 SST changes, *red* symbols represent experiments prescribing Cluster 3 SST changes. *Red lines* show linear regressions, which are only drawn in panels for which the correlation coefficient is positive and statistically significant at the 90% level according to Pearson's product-moment correlation significance test

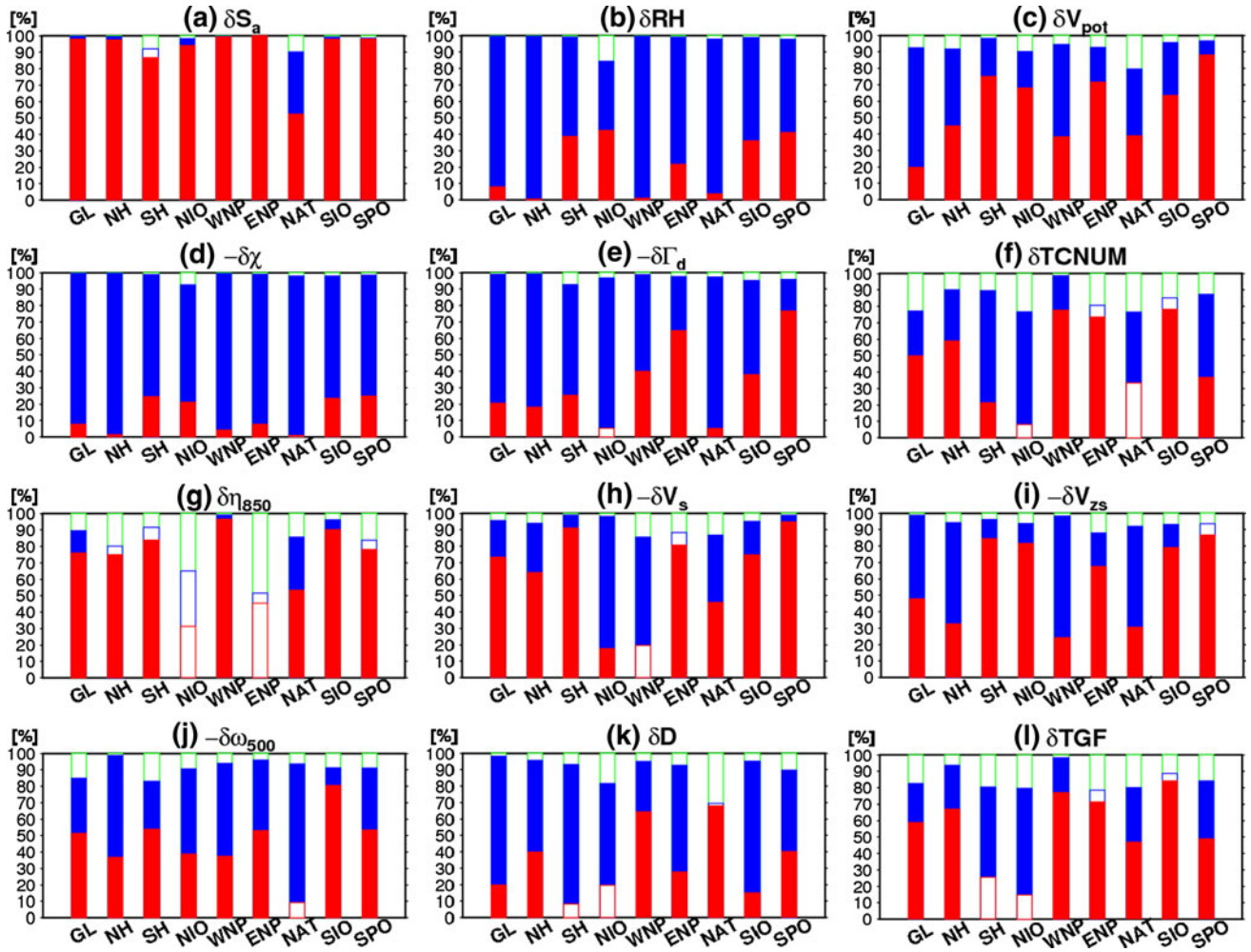

Fig. 9 The fractional rate of variance [%] relative to total variance that arises from use of different prescribed SST change (*red*), use of different cumulus convection scheme (*blue*), and residual (*green*) computed by a two-way analysis of variance (ANOVA) without replication. *Filled colour bars* indicate elements that are significantly affected by the factor (difference in SSTs or cumulus schemes) at the 90% significance level according to the *F* test applied in ANOVA, while *open colour bars* indicate elements that are not significantly affected by the factor

number. This result holds both at ocean-basin scales and the global and hemispheric scales.

4 Conclusion and discussions

The 60-km-mesh MRI-AGCM (v3.2) was used to generate ensemble simulations of the present-day (1979–2003, control) and the end of 21st century (2075–2099) climates under the IPCC A1B scenario to investigate uncertainties in projected future changes in TC activity at global and ocean-basin scales. The simulations were conducted using three different cumulus convection schemes (the Yoshimura scheme, YS; the Kain–Fritsch scheme, KF; and the Arakawa–Schubert scheme, AS). Future SSTs were prescribed either as the ensemble mean of 18 CMIP3 models or as one of three different SST spatial patterns determined by a cluster analysis of the CMIP3 models.

Results for the control simulations using all three cumulus convection schemes demonstrate that the climatological global distributions of TCs compare reasonably well with observations, although TC genesis numbers simulated at the basin scale by the control simulation using the AS scheme are more heavily biased relative to observations than the control simulations using the other cumulus convection schemes. All three configurations of the model underestimate TC genesis number in the North Atlantic (NAT) and overestimate TC genesis number in the Southern Hemisphere (SH); these biases should be taken into account when evaluating projected future changes in TC activity.

Regardless of differences in model cumulus convection schemes and prescribed SSTs, all ensemble simulations

robustly project decreases in global and hemispheric TC genesis numbers by approximately 5%–35% under the global warming environment. Moreover, all experiments tend to project future decreases in the number of TCs in the western North Pacific (WNP), South Indian Ocean (SIO), and South Pacific Ocean (SPO). The projected changes in the NAT, North Indian Ocean (NIO), and eastern North Pacific (ENP) are inconsistent in both amount and sign among the experiments.

Most of the future experiments consistently indicate reductions in both projected TC frequency (TCF) and TC genesis frequency (TGF) over the western portion of WNP, SIO, and SPO, and increases in TCF and TGF over the central Pacific. The degree of the projected future increases in TGF in the central Pacific correlate well with the prescribed SST anomaly, which is defined as the local SST change subtracted from the tropical mean (30°S–30°N) change. An additional experiment, for which SST are prescribed as a globally uniform increase of 1.83 K relative to the present-day, projects a similar spatial pattern of future changes in TGF to that projected by the multi-ensemble mean. This result indicates that the spatial contrast in projected future changes in TGF between the WNP and the central Pacific is primarily due to the underlying global warming. This appears to be the result of a weakening of the Walker circulation; this weakening has been reported by multiple previous studies (e.g., Vecchi and Soden 2007a). We speculate that spatially inhomogeneous changes in SST anomalies act to modify the underlying spatial pattern of changes in TGF that result from the global warming effect.

Changes in dynamical and thermodynamic large-scale parameters were also investigated to better identify the factors responsible for differences in projected future changes in TGF among the ensemble experiments. Variability in projected future changes in global TGF among the ensemble simulations appears to primarily result from differences in the SST anomaly. Large-scale parameters such as lower tropospheric relative vorticity, vertical wind shear, vertical pressure–velocity at 500 hPa, and variance in synoptic-scale disturbances appear to also influence projected future changes in TGF at regional scales; however, thermodynamic parameters, such as relative humidity at 700 hPa, saturation deficit at 700 hPa, and static stability, do not appear to be a major factor. These thermodynamic parameters tend to depend on the selected cumulus convection scheme, while the dynamical parameters are more dependent on the prescribed SSTs. These results suggest that uncertainties in the degree of projected future change in TGF and TC genesis number are more attributable to difference in SST spatial patterns than to differences in model physics. Additional SST ensemble experiments may be needed to reduce these uncertainties.

Model biases in the control simulations could be inherited by the projections of the future changes. Reducing uncertainties will therefore require minimising these biases. Our experiments have not considered coupled atmosphere–ocean interactions, which are an important component of TC genesis. We have also only considered differences in the cumulus convection schemes for differences in model physics. TC genesis may be sensitive to a number of other parameters and parameterizations, so that different configurations of the multi-model ensemble may yield results that are different from those we have reported here.

Acknowledgments This work was conducted under the framework of the "Projection of the Change in Future Weather Extremes using Super-High-Resolution Atmospheric Models" project supported by the KAKUSHIN programme of the Ministry of Education, Culture, Sports, Science, and Technology (MEXT) of Japan. Calculations were performed on the Earth Simulator.

References

Arakawa A, Schubert WH (1974) Interaction of cumulus cloud ensemble with the large-scale environment. Part I. J Atmos Sci 31:674–701

Bengtsson L, Botzet M, Esch M (1996) Will greenhouse gas-induced warming over the next 50 years lead to higher frequency and greater intensity of hurricanes? Tellus 48A:57–73

Bengtsson L, Hodges KI, Esch M, Keenlyside N, Kornblueh L, Luo J-J, Yamagata T (2007) How may tropical cyclones change in a warmer climate? Tellus 59A:539–561

Ding Y, Sikka DR (2006) Synoptic systems and weather. In: Wang B (ed) The Asian monsoon. Springer, Berlin, pp 131–201

Emanuel K (1987) The dependence of hurricane intensity on climate. Nature 326:483–485

Emanuel KA (1995) Sensitivity of tropical cyclones to surface exchange coefficients and a revised steady-state model incorporating eye dynamics. J Atmos Sci 52:3969–3976

Emanuel K (2008) Hurricanes and global warming. Bull Am Meteor Soc 89:347–367

Emanuel KA, Nolan DS (2004) Tropical cyclone activity and global climate. Preprints. 26th Conf on hurricanes and tropical meteorology. Miami, FL, Amer Meteor Soc, pp 240–241

Gill AE (1980) Some simple solutions for heat-induced tropical circulation. Quart J Roy Meteorol Soc 106:447–462

Gray WM (1968) Global view of the origin of tropical disturbances and storms. Mon Weather Rev 96:669–700

Held IM, Zhao M (2011) The response of tropical cyclone statistics to an increase in CO_2 with fixed sea surface temperature. J Clim 24:5353–5364

IPCC (2007) Climate change 2007: the physical science basis. Contribution of working group I to the fourth assessment report of the intergovernmental panel on climate change. Cambridge University Press, Cambridge, p 996

Kain JS, Fritsch JM (1990) A one-dimensional entraining/detraining plume model and its application in convective parameterization. J Atmos Sci 47:2784–2802

Kain JS, Fritsch JM (1993) Convective parameterization for mesoscale models: the Kain–Fritsch scheme. In: Emanuel KA, Raymond DJ (eds) The representation of cumulus convection in numerical models of the atmosphere. Meteorology Monographs No 46. Am Meteor Soc, pp 165–170

Knutson T, McBride JL, Chan J, Emanuel K, Holland G, Landsea C, Held I, Kossin JP, Srivastava AK, Sugi M (2010) Tropical cyclones and climate change. Nat Geosci 3:157–163

Lau K-H, Lau N-C (1990) Observed structure and propagation characteristics of tropical summertime synoptic-scale disturbances. Mon Weather Rev 118:1888–1913

Li T (2006) Origin of the summertime synoptic-scale wave train in the western North Pacific. J Atmos Sci 63:1093–1102

Li T (2011) Synoptic and climatic aspects of tropical cyclogenesis in western North Pacific. In: Oouchi K, Fudeyasu H (eds) Cyclones: formation, triggers and control. Noval Science Publishers, New York

Li T, Kwon M, Zhao M, Kug J-S, Luo J-J, Yu W (2010) Global warming shifts Pacific tropical cyclone location. Geophys Res Lett 37:L21804

Mizuta R, Adachi Y, Yukimoto S, Kusunoki S (2008) Estimation of the future distribution of sea surface temperature and sea ice using the CMIP3 multi-model ensemble mean. Tech Rep Meteor Res Inst 56:28 [available at http://www.mri-jma.go.jp/Publish/Technical/DATA/VOL_56/56.html]

Mizuta R, Yoshimura H, Murakami H, Matsueda M, Endo H, Ose T, Kamiguchi K, Hosaka M, Sugi M, Yukimoto S, Kusunoki S, Kitoh A (2012) Climate simulations using MRI-AGCM with 20-km grid. J Meteor Soc Jpn 90A:235–260

Murakami H, Sugi M (2010) Effect of model resolution on tropical cyclone climate projections. SOLA 6:73–76

Murakami H, Wang B (2010) Future change of North Atlantic tropical cyclone tracks: projection by a 20-km-mesh global atmospheric model. J Clim 23:2699–2721

Murakami H, Wang B, Kitoh A (2011) Future change of western North Pacific typhoons: projections by a 20-km-mesh global atmospheric model. J Clim 24:1154–1169

Murakami H, Wang Y, Sugi M, Yoshimura H, Mizuta R, Shindo E, Adachi Y, Yukimoto S, Hosaka M, Kitoh A, Ose T, Kusunoki S (2012) Future changes in tropical cyclone activity projected by the new high-resolution MRI-AGCM. J Clim 25:3237–3260

Oouchi K, Yoshimura J, Yoshimura H, Mizuta R, Kusunoki S, Noda A (2006) Tropical cyclone climatology in a global-warming climate as simulated in a 20 km-mesh global atmospheric model: Frequency and wind intensity analysis. J Meteor Soc Jpn 84:259–276

Randall D, Pan D-M (1993) Implementation of the Arakawa–Schubert cumulus parameterization with a prognostic closure. The representation of cumulus convection in numerical models. Meteor Monogr Am Meteor Soc 46:137–144

Rayner NA, Parker DE, Horton EB, Folland CK, Alexander LV, Rowell DP (2003) Global analysis of sea surface temperature, sea ice, and night marine air temperature since the late nineteenth century. J Geophys Res 108:4407

Storch HV, Zwiers FW (1999) Analysis of variance. In: Storch HV, Zwiers FW (eds) Statistical analysis in climate research. Cambridge University Press, Cambridge, pp 171–192

Stowasser M, Wang Y, Hamilton K (2007) Tropical cyclone changes in the western North Pacific in a global warming scenario. J Clim 20:2378–2396

Sugi M, Noda A, Sato N (2002) Influence of the global warming on tropical cyclone climatology: an experiment with the JMA global model. J Meteor Soc Jpn 80:249–272

Sugi M, Murakami H, Yoshimura J (2009) A reduction in global tropical cyclone frequency due to global warming. SOLA 5:164–167

Tiedtke M (1989) Acomprehensive mass flux scheme for cumulus parameterization in large-scale models. Mon Wea Rev 117:1779–1800

Unisys (2012) Unisys weather hurricane tropical data. [Available online at http://weather.unisys.com/hurricane/]

Vecchi GA, Soden BJ (2007a) Global warming and the weakening of the tropical circulation. J Clim 20:4316–4340

Vecchi GA, Soden BJ (2007b) Increased tropical Atlantic wind shear in model projections of global warming. Geophys Res Lett 34:L08702. doi:10.1029/2006GL028905

Walsh KJE, Fiorino M, Landsea CW, McInnes KL (2007) Objectively determined resolution-dependent threshold criteria for the detection of tropical cyclones in climate models and reanalyses. J Clim 20:2307–2314

Walsh K, Lavender S, Murakami H, Scoccimarro E, Caron L-P, Ghantous M (2010) The tropical intercomparison project. In: Elsner JB, Hodges RE, Malmstadt JC, Scheitlin KN (eds) Hurricanes and climate change. Springer, Berlin, pp 1–24

Wang B, Xie X (1996) Low-frequency equatorial waves in vertically sheared zonal flow. Part I: stable waves. J Atmos Sci 53:449–467

Wilks DS (2006) Cluster analysis. In: Wilks DS (ed) Statistical methods in the atmospheric sciences, 2nd edn. Academic Press, London, pp 549–562

Xie S-P, Deser C, Vecchi GA, Ma J, Teng H, Wittenberg AT (2010) Global warming pattern formation: sea surface temperature and rainfall. J Clim 23:966–986

Yokoi S, Takayabu YN (2009) Multi-model projection of global warming impact on tropical cyclone genesis frequency over the western North Pacific. J Meteor Soc Jpn 87:525–538

Yokoi S, Takayabu YN, Chan JCL (2009) Tropical cyclone genesis frequency over the western North Pacific simulated in medium resolution coupled general circulation models. Clim Dyn 33:665–683

Yukimoto S et al. (2011) Meteorological research institute-earth system model v1 (MRI-ESM1)—model description. Tech Rep Meteor Res Inst 64, p 88 [available at http://www.mri-jma.go.jp/Publish/Technical/DATA/VOL_64/index.html]

Zhao M, Held IM, Lin S-J, Vecchi GA (2009) Simulations of global hurricane climatology, interannual variability, and response to global warming using a 50 km resolution GCM. J Clim 22:6653–6678

Zhao M, Held IM, Vecchi G (2010) Retrospective forecasts of the hurricane season using a global atmospheric model assuming persistence of SST anomalies. Mon Wea Rev 138:3858–3868